Nanoscale

RSC Publishing

PAPER

View Article Online
View Journal | View Issue

Phonon spectroscopy in a Bi_2Te_3 nanowire array

Cite this: *Nanoscale*, 2013, **5**, 10629

Dimitrios Bessas,†[ab] William Töllner,[c] Zainul Aabdin,[d] Nicola Peranio,[d] Ilya Sergueev,‡[e] Hans-Christian Wille,[f] Oliver Eibl,[d] Kornelius Nielsch[c] and Raphaël P. Hermann*[ab]

Received 5th June 2013
Accepted 15th August 2013

DOI: 10.1039/c3nr02918b

www.rsc.org/nanoscale

The lattice dynamics in an array of 56 nm diameter Bi_2Te_3 nanowires embedded in a self-ordered amorphous alumina membrane were investigated microscopically using ^{125}Te nuclear inelastic scattering. The element specific density of phonon states is measured on nanowires in two perpendicular orientations and the speed of sound is extracted. Combined high energy synchrotron radiation diffraction and transmission electron microscopy was carried out on the same sample and the crystallinity was investigated. The nanowires grow almost perpendicular to the *c*-axis, partly with twinning. The average speed of sound in the 56 nm diameter Bi_2Te_3 nanowires is ~7% smaller with respect to bulk Bi_2Te_3 and a decrease in the macroscopic lattice thermal conductivity by ~13% due to nanostructuration and to the reduced speed of sound is predicted.

1 Introduction

Theoretical foundations of nanoscale systems exist[1] and are routinely used to predict enhancement in thermal,[2] electrical,[3] and mechanical[4] properties of the investigated systems. Recently, owing to rapid progress in nanostructuration technology the attention of the scientific community was drawn anew to the microscopic characterisation of low dimensional structures. Among the nanoscale systems, 2D nanomaterials such as graphene[5] and transition metal oxide nanolayers[6] are of great technological importance. The traditional 2D nanomaterials[7] have a thickness on the order of a few nanometers and length on the order of microns which makes them candidates not only for direct applications but also as building blocks of artificial structures.

In 1993, Hicks and Dresselhaus[8,9] predicted a significant enhancement in the thermoelectric figure of merit,[10] zT, due to the effective mass of charge carriers both in two- and one-dimensional nanostructures below $d = 3$ nm, where d is the dimension of confinement. After this prediction a great number of experimental studies were dedicated to the realisation of the asymptotic d^{-2} enhancement of zT. Soon after, phonon confinement effects were proposed in the thermal–thermoelectric context.[11–13] However, a definitive experimental confirmation is nevertheless still lacking. In a recent theoretical study Cornett and Rabin[14] have investigated the electrical properties of semiconducting nanowires but no clear enhancement of the electrical properties was suggested for nanowires with several nanometers diameter. Arguably, the electronic mean free path is orders of magnitude shorter than that of phonons, thus in the first approximation no clear effect of electronic properties is expected for $d \sim 100$ nm.[15–17]

Tetradymite structured chalcogenides exhibit, in addition to good thermoelectric conversion properties, a reversible phase change from crystalline to amorphous phase induced by temperature or an electric field.[18,19] Because the phase change is accompanied by a large resistance or reflectivity change such materials are considered candidates for future nonvolatile memory applications.[20] When such chalcogenides are used in phase change applications[21] their thermal conductivity plays an important role as it ultimately limits the read–write time. Hence, tailoring the macroscopic properties of these materials by tuning their dimensions is not only of importance for fundamental reasons but also has a potential impact in information technology and power conversion.

Previous studies of thermal transport in nanowires with diameter in the range of several nanometers revealed phonon confinement due to nanostructuration[22,23] as well as by surface roughness.[24] Finite size effects were predicted to cause a significant frequency shift or a lineshape broadening[25] for the phonon modes. Nevertheless, misleading artifacts of instrumental origin resulting in such effects were identified and explained in germanium nanowires.[26] To the best of our knowledge, no complete experimental study exists on the density of phonon states in nanowires due to experimental

[a]*Jülich Center for Neutron Science JCNS, Peter Grünberg Institut PGI, JARA-FIT, Forschungszentrum Jülich GmbH, D-52425 Jülich. E-mail: r.hermann@fz-juelich.de; Fax: +49 2461 61 2610; Tel: +49 2461 61 4786*

[b]*Faculté des Sciences, Université de Liège, B-4000, Liège*

[c]*Institute of Applied Physics, University of Hamburg, Jungiusstr. 11, D-20355 Hamburg*

[d]*Institut für Angewandte Physik, Eberhard Karls Universität Tübingen, D-72076 Tübingen*

[e]*European Synchrotron Radiation Facility, F-38043 Grenoble*

[f]*Deutsches Elektronen-Synchrotron, D-22607 Hamburg*

† Present address: European Synchrotron Radiation Facility, F-38043 Grenoble, France.

‡ Present address: Deutsches Elektronen-Synchrotron, D-22607 Hamburg, Germany.

limitations. The limited amount of material and the complexity in handling, makes inelastic X-ray scattering probably currently the only choice for investigating microscopically the lattice dynamics, and more precisely the density of phonon states of oriented nanowires.

The phonon properties in an ensemble of 56 nm diameter nanowires embedded in a self-ordered amorphous alumina membrane are the focus of this study. The lattice dynamical characterization was based on nuclear resonance inelastic scattering[27] using the ^{125}Te resonance.[28] In order to enable correct mode attribution and complement the dynamical properties in the nanowire ensembles a combined detailed structural characterization was conducted using both high energy synchrotron radiation and electron scattering. According to our results a possible reduction in thermal conductivity should primarily be related to the reduced speed of sound as no measurable mode broadening is observed.

2 Materials and methods

We prepared ^{125}Te enriched Bi_2Te_3 nanowires, NW, embedded in an anodic self-ordered alumina membrane[29] using a novel pulsed electrodeposition technique described elsewhere.[30] In this work, the alumina membrane had a nominal pore diameter of 50 nm with a nominal interpore distance of 100 nm. The aqueous electrodeposition solution was formed by dissolution of bismuth(III) nitrate pentahydrate and 80% ^{125}Te enriched tellurium powder in the appropriate ratio. Based on previous studies,[31] the reduction potential was set to −200 mV in fixed pulses of 10 ms and the relaxation potential to 80 mV for 50 ms. All measurements reported in this study were carried out on small fragments taken from the same alumina membrane, see Fig. 1a.

In order to verify the crystallographic phase, diffraction using synchrotron radiation was performed at the 6-ID-D station of the Advanced Photon Source on bundles of nanowires inside the intact template. Measurements were carried out at 295 K in two orientations, (i) with the incident k vector parallel to the nanowire axes, called transmission geometry and (ii) with the incident k vector perpendicular to the nanowire axes, called grazing incidence geometry. Data were collected using an amorphous Si area detector of 2048 × 2048 pixels (pixel size: 200 μm). The wavelength was 0.142519 Å and the sample detector distance of 1715.5 mm was calibrated using diffraction from NIST Si 470c. The reflection positions were extracted after fitting the data with a Lorentzian profile. Both detector patterns should be interpreted as follows: the radial distance from the beam center corresponds to the scattering angle 2θ and the circular angle at certain radius corresponds to the azimuthal angle ϕ. Thus, apart from typical information related to structural properties, insight in preferential wire growth was obtained. From both detector patterns the one dimensional diffractograms were extracted after radially integrating the intensities at all azimuthal angles for a certain 2θ. In order to understand our raw data of the detector images the texture simulation program Anaelu[32] was used and a rotational system composed of three angles, namely x, y, z, around the corresponding coordinate system was introduced.

Structure and chemical composition of single nanowires for the same sample were characterized by Scanning and Transmission Electron Microscopy (SEM and TEM). For TEM analysis, the alumina matrix was selectively dissolved using a mixture of 6 wt% H_3PO_4 and 1.8 wt% H_2CrO_4 for several days at 40 °C. The nanowire suspension was deposited on holey grids and dried at room temperature.

A Zeiss 912 Ω TEM with a LaB_6 gun was used and operated at 120 kV. Crystallinity and grain orientation were analyzed by electron diffraction patterns for which a Selected Area Electron Diffraction, SAED, aperture was used selecting regions with a diameter of 750 nm.[31,33] The size of the crystallites was determined by bright- and dark-field images of nanowires under two-beam diffraction conditions.[31] The chemical composition was

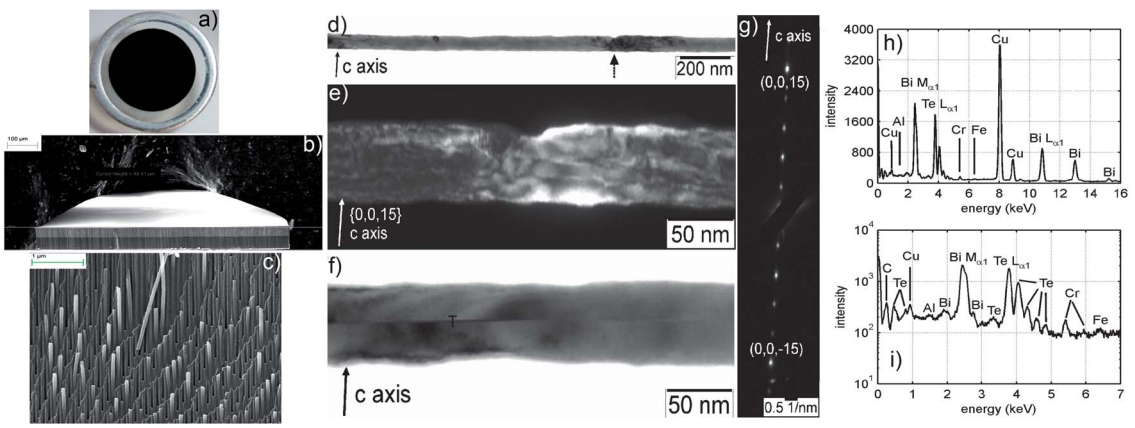

Fig. 1 (a) The alumina membrane (transparent area) inside an aluminium frame filled with Bi_2Te_3 nanowires (dark area). (b) A cross-section of the alumina membrane. (c) Low magnification SEM image by a fragment of the alumina membrane which shows the quality and uniformity of nanowires. (d) Overview of a TEM bright-field image. (e) High-magnification dark-field TEM image obtained with strongly excited reflections {0 0 15}, acquired at the nanowire region indicated by a dashed arrow in (d). (f) TEM bright field image of another nanowire with the twin boundary parallel to the basal plane in the center. (g) Appropriately rotated electron diffraction pattern obtained on the nanowire shown in (d). EDX spectrum acquired in the TEM on a Bi_2Te_3 nanowire with a Te mole fraction of 64.4 at.%, shown in (h) linear and (i) logarithmic scales.

analyzed by energy-dispersive X-ray spectrometry, EDX, in the TEM. Details of the spectral resolution, lateral resolution, acquisition conditions, and accuracy of quantitative chemical analysis by EDX were described elsewhere.[31,34]

The diameter and chemical composition of the single nanowires were also measured in a SEM combined with EDX spectrometry with an accuracy of 0.5 at.% using bulk Bi_2Te_3 calibration standards. Chemical analysis by EDX in the SEM was in agreement with TEM.

The lattice dynamics were investigated by means of Nuclear resonance Inelastic Scattering, NIS, using a backscattering sapphire single crystal monochromator[28,35] with a resolution of 1.1 meV for, 35.49 keV, ^{125}Te resonance. Several spectra, on the same sample and orientation for which diffraction patterns were acquired, were recorded in 16-bunch mode at the nuclear resonance station ID18 (ref. 36) of the European Synchrotron Radiation Facility. In order to minimise multiphonon contributions the measurements were carried out at 40 K. The elastic peak in the spectra was subtracted and a modified version of the program DOS[37] for reconvoluting the extracted Density of Phonon States, DOS, with a Gaussian profile with the same Full Width at Half Maximum, FWHM, as the measured time integrated NFS was used to extract the density of phonon states. The self-consistency of the procedure was confirmed by applying the conventional sum rules.[38] The DOS in transmission geometry shows enhanced statistical noise and increased errorbar compared to grazing incidence geometry due to the limited amount of material defined by the nanowire length.

3 Results

3.1 Morphology and crystallinity

It was found that the average wire length was 16 μm and appeared relatively homogeneous with no hint of overgrowth of the template pores as well as surface roughness, see Fig. 1.

The diameters of the nanowires were determined by TEM and varied between 53 and 59 nm, in agreement with SEM analysis. Fig. 1g shows an electron diffraction pattern of a wire in a pole orientation (Fig. 1d). The {0 0 *l*} reflections are clearly seen and an angle of 85° between the crystallographic *c*-axis and the nanowire axis was determined. Electron diffraction patterns observed at different points of single nanowires[33] revealed single crystallinity over a length of 15 μm. In addition to single crystalline nanowires, see Fig. 1e, twinned nanowires coming from the same template were observed with the twinning plane located at the center of the nanowire, see Fig. 1f.

The precise chemical composition was measured by EDX in the TEM. Fig. 1h and 1i show the expected Bi and Te lines and in addition Cu, Fe, C, Cr, and Al X-ray lines. The additional X-ray lines are coming either from well-known instrumental artifacts,[34] *i.e.* Cu, Fe and C, or from dissolving the alumina template, *i.e.* Cr and Al. An oxygen peak was not observed and therefore there is no sign of surface oxidation. EDX spectra were acquired on several nanowires and average Te and Bi mole fractions of 64.6 at.% and 35.4 at.% were determined, respectively.

X-ray diffraction by a fragment of the alumina template filled with Bi_2Te_3 nanowires was obtained in two perpendicular orientations. Note that because the template is amorphous no contribution is expected in the diffractograms. Fig. 2a and c show the detector patterns in circular coordinates obtained in both orientations. For the sake of simplicity half a detector image is shown. The diffraction patterns in both orientations

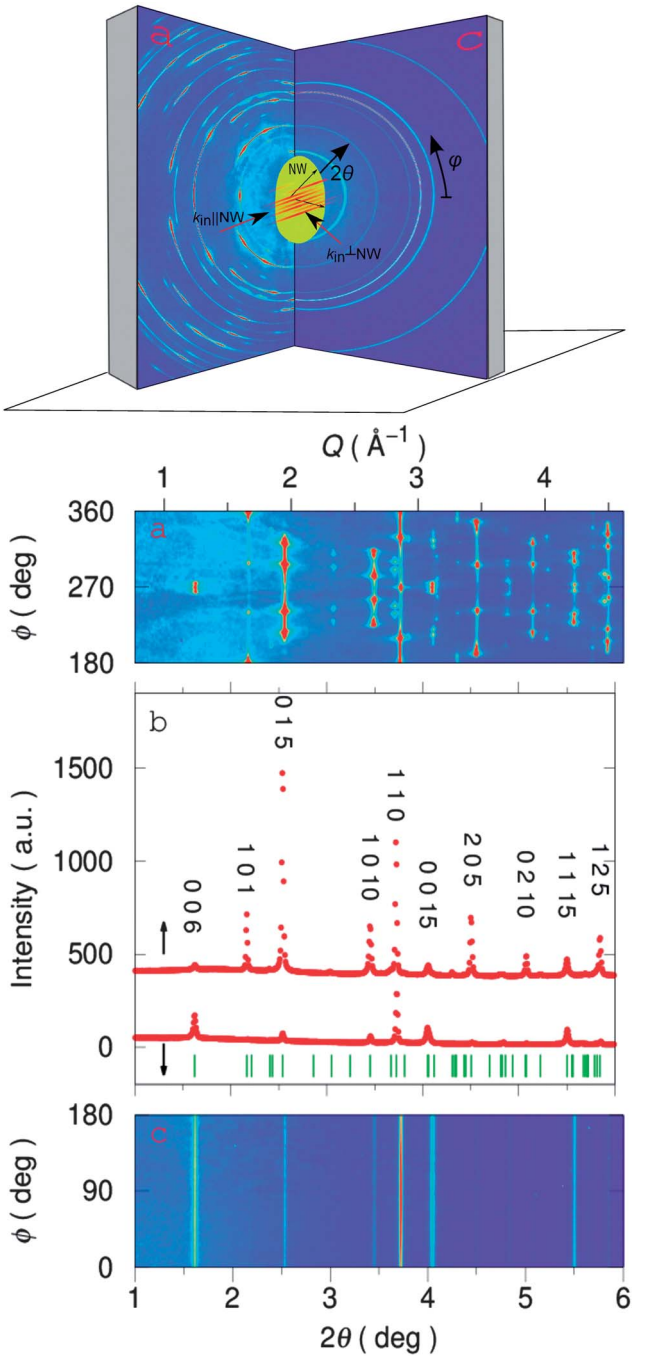

Fig. 2 Diffraction of synchrotron radiation obtained on an array of Bi_2Te_3 nanowires embedded in a self-ordered amorphous alumina membrane. Top: the diffraction configuration. (a) The pattern recorded using a two dimensional area detector in grazing incidence geometry *versus* the azimuthal angle ϕ. (c) The azimuthal projection of the Debye–Scherrer rings measured in transmission geometry. (b) The extracted diffractograms (red points).

are indicative of a rhombohedral lattice ($R\bar{3}m$, #160). The lattice parameters obtained at 295 K are a = 4.3824(1) Å and c = 30.2588(1) Å. Although the lattice parameter along the a-axis is in excellent agreement with that of bulk Bi_2Te_3,[39] the lattice parameter along the c-axis appears ~1% reduced compared to the bulk. In transmission geometry the observed Debye–Scherrer rings reveal azimuthally isotropic scattering. In grazing incidence geometry a strongly anisotropic intensity distribution is observed. The detector pattern appears highly symmetric with a mirror plane around 270°. For the (0 0 6) reflection a triplet of equal intensity peaks at 264.5(1)°, 269.8(1)° and 275.2(1)° is observed. Even with the additional information of unit cell twinning the reflection indexing of our detector pattern, see Fig. 2a, using only the interplanar angles between the detected reflections and the (0 0 6) reflection appears puzzling. For example, the nominal angles between the {0 0 l} and the (1 0 1) or the (0 1 5) type of reflections are 82.9° and 58.1°, respectively. However, in our diffraction pattern additional reflections with different azimuthal angles belonging to (1 0 1) and (0 1 5) types of reflections are visible. In diffraction of high energy synchrotron radiation, due to very large attenuation length, *i.e.* ~700 μm at 86.9 keV, a superposition of diffraction patterns is obtained from different single crystalline nanowires embedded in the same template. In grazing incidence geometry, the c-axis was found almost perpendicular, between 89 and 91° relative to the nanowire axis. The detector pattern in transmission geometry indicates that the (0 0 6) reflection is isotropically distributed in the scattering plane, see Fig. 2c.

In summary, the array of 56 nm diameter and 16 μm long Bi_2Te_3 nanowires embedded in an amorphous alumina membrane exhibits a complex diffraction pattern due to preferred orientation during sample growth as well as due to twinning which might be related either to chemical composition or effective conditions during electrodeposition. The nanowire growth is along the ⟨1 0 1⟩ direction and the c-axis is within 5° perpendicular to the wire axis. The nanowire array shows a powder like diffraction pattern in one orientation and a composite single crystal like diffraction pattern in the perpendicular one. It, thus, gives us the possibility to study the influence of phonon transport due to nanostructuration and to clarify preferred orientation issues on the same sample.

3.2 Lattice dynamics

The nuclear inelastic scattering spectra and the density of phonon states from ^{125}Te enriched bulk ceramics and single crystalline Bi_2Te_3 have been reported earlier.[40] The ^{125}Te specific projected DOS, $g(E)$, on the nanowire ensemble extracted in both orientations, *i.e.*, transmission and grazing incidence geometry, are shown in Fig. 3. In NIS only vibrations of the resonant nuclei along the direction of the incident beam are recorded.[41] In isotropic materials the direction dependent information is lost, however, in single crystals of anisotropic materials phonon polarization analysis can be carried out, *e.g.* as was done[40] in bulk Bi_2Te_3.

For a given propagation direction there are two transversely and one longitudinally polarized modes per atom in the

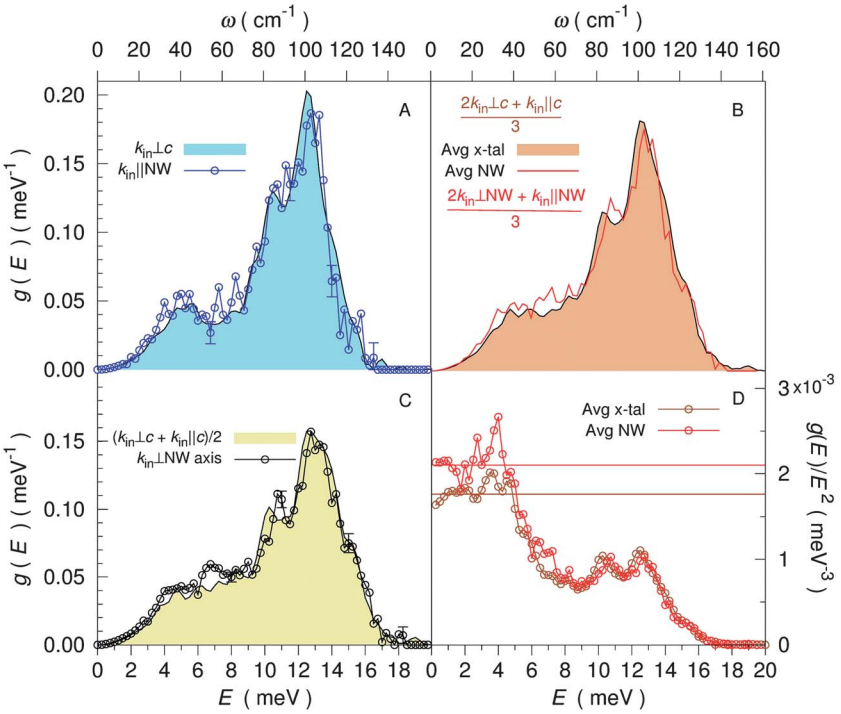

Fig. 3 Te specific DOS measured in two geometries, (panel A) with the incident beam parallel (blue points) and (panel C) perpendicular (black points) to an array of Bi_2Te_3 nanowires. Typical error bars are given. For comparison, reference data[40] (highlighted areas) measured on a Bi_2Te_3 single crystal are depicted. In panel B the averaged DOS in Bi_2Te_3 NW and a single crystal are depicted. Panel D shows the Debye representation, $g(E)/E^2$, and the extracted Debye level (color lines), $\lim_{E\to 0} g(E)/E^2$ for data depicted in panel B.

primitive unit cell and, conversely, for a given phonon polarization there are two transverse and one longitudinal modes. Specifically, when the incident beam is parallel to the NW axis, *i.e.*, $k_{in} \| NW$, and the crystallographic *c*-axis is distributed isotropically perpendicular to the NW then the measured spectra correspond to the DOS perpendicular to the crystallographic *c*-axis, *i.e.* $DOS^{kin \perp c}$. In case the incident beam is perpendicular to the NW axis, *i.e.*, $k_{in} \perp NW$, the measured DOS is $(DOS^{kin \perp c} + DOS^{kin||c})/2$. Hence, in order to extract the $DOS^{kin||c}$ we have to use the formula $DOS^{kin||c} = 2DOS^{kin||NW} - DOS^{kin \perp NW}$. Both $DOS^{kin \perp c}$ and $DOS^{kin||c}$ extracted from NIS data on Bi_2Te_3 nanowire ensembles as well as comparison to the corresponding single crystal data[40] are shown in Fig. 3. We averaged our orientation dependent DOS obtained on NW and compared it with the one extracted on a similar single crystal. All features in both DOS essentially match.

From the DOS a series of thermodynamical parameters can be obtained.[42] The Te specific mean force constant, $\langle F_i \rangle$, is obtained from the expression $\langle F_i \rangle = m_R \int_0^\infty g(E)E^2 dE/\hbar^2$, where m_R is the resonant nuclear mass. The obtained value, 59(1) N m^{-1}, is practically the same with the one obtained earlier[40] on bulk Bi_2Te_3, *i.e.* 58(1) N m^{-1}. The speed of sound, v_s, is obtained, in the Debye approximation, from the long wavelength vibrational modes – herein assumed as $E < 4$ meV or $\lambda \geq 3$ Å. Fig. 3D shows the average Debye level, $\lim_{E \to 0} g(E)/E^2$, in the nanowire array as compared to bulk samples. The average Debye level in 56 nm diameter nanowires increases by ~19(2)%, by 312(2)% for vibrations along the *c*-axis and by ~13(1)% for vibrations along the *a*-axis. The average speed of sound can be extracted by using the formula,[43] $\lim_{E \to 0} g(E)/E^2 = m_R/2\pi^2\hbar^3\rho v_s^3$, where ρ is the mass density. Having almost the same mass density in the case of a bulk single crystal and single crystalline nanowires, the extracted average speed of sound in NW decreases by 6.5(1)%.

4 Discussion

The binary system Bi_xCh_y (Ch = Te or Se) displays several phases in the compositional range between 40 and 70 at.% Bi.[44] This wide variation of chemical composition has been theoretically explained in Bi_xSe_y by the approximately zero formation energy difference between all phases.[45] Remarkably, all Bi_xTe_y phases crystallise in rhombohedral symmetry with a very similar in-plane lattice parameter, *a*, however, the out-of-plane lattice parameter, *c*, is distinctive.[46] This effect is confirmed by our measurements and only the lattice constant along the *c*-axis appears ~1% reduced compared to the bulk counterpart.

The chemical composition does not only affect the phase in which the material crystallizes but also the sample treatment, *e.g.* shear deformation during hot-pressing[3] is a key factor. In this study, we identified twins by TEM on several wires formed during sample growth. The twinning plane corresponds to 180° rotation of the unit cell around the *c*-axis.[47] A similar twinning plane has been reported earlier by Medlin *et al.*[48] on Bi_2Te_3 nanocomposite samples prepared using current assisted sintering, however, the precise chemical composition after sintering is not given. Thus, we can attribute the formation of twins neither to off stoichiometry nor to sample growth conditions.

The influence of defects and doping on the phonon lifetime of optical phonons has been studied in carbon nanotubes.[49] The shift of the vibrational mode around 13 meV between grazing incidence geometry and transmission geometry is attributed to geometrical effects, *i.e.* probing of different phonon modes in the Brillouin zone. This is substantiated by our averaged DOS obtained on NW and its comparison to the one obtained on a similar single crystal where such a shift is not present. However, a moderate decrease in the speed of sound by 6.5% has been observed in the long wavelength-low energy-limit between our nanowires at 40 K and bulk samples measured at 20 K. Temperature effects do not alter significantly the elastic constants[50] of bulk Bi_2Te_3 between 20 and 40 K and thus practically no change in the speed of sound is expected at such low temperatures. Hence, the observed difference in the speed of sound between bulk and Bi_2Te_3 nanowires is solely attributed to confinement due to nanostructuration.

In this study the NW were embedded in an amorphous alumina template. Semiconducting NW with lateral dimensions in the range of few nanometers, *i.e.* GaN, covered with barrier coatings with higher – *e.g.* AlN- or lower – *e.g.* plastic-sound velocities with respect to the NW have been studied theoretically by Balandin *et al.*[51] It was found that acoustically softer coatings lead to strong reduction of the phonon group velocities whereas the acoustically stiffer coatings increased the group velocity of NW. In our case, the NW have diameter of 56 nm and are embedded in an acoustically harder amorphous alumina membrane. According to a recent theoretical investigation of such templates[52] the Debye law is preserved until 20 meV where the first phonon peak appears. The optical modes of the template rise between 24 and 120 meV. The speed of sound in the alumina membrane, 6.76 km s^{-1}, is almost four times larger than in bulk Bi_2Te_3, 1.75 km s^{-1}. One might reasonably expect that the acoustic part in the density of phonon states of the embedded nanowires is stiffer than for the free standing nanowires. The relevant energy scale for observing strong template/wire interactions can be estimated using the diameter and the speed of sound as $E = h/(1500\ m\ s^{-1}) \times 50\ nm \sim 120\ \mu eV$ and is presently inaccessible by our method, although within reach for future inelastic neutron scattering studies. The alumina template in this case is considered to behave as an isotropic elastic medium without interference with the bismuth telluride phonons.

Note that although phonon interactions between the template and NW are practically not taking place in the observed energy range, the thermal conductivity at room temperature of the alumina template,[53] 1.3 W m^{-1} K^{-1}, is in the same range like the thermal conductivity measured on similar Bi_2Te_3 nanowires[54] and thus direct integration of nanowires in functional devices inside the template is not desirable because of the additional heat leakages.

Thermal conductivity data on bulk polycrystalline and single crystalline Bi_2Te_3 have been measured and show not only a variation as a function of Te composition[55] due to electronic part of thermal conductivity but also significant variations for different crystallographic orientations, *i.e.* the lattice thermal conductivity in Bi_2Te_3 is almost 3 times larger when measured perpendicular than parallel to crystallographic *c*-axis.[56] Thus,

slight off-stoichiometry does not significantly influence the lattice part of the thermal conductivity as much as the crystallographic orientation does.

Nuclear inelastic scattering does not directly study phonon transport, however, it does provide direct access to the element specific density of phonon states from which all essential macroscopic properties, such as heat capacity or the speed of sound, related to phonon transport can be accessed except for the phonon mean free path. In the first approximation, the lattice thermal conductivity, k_L, depends on the specific heat at constant volume, C_V, the sound velocity, v_s, and the phonon lifetime, τ, and can be expressed by the simple kinetic gas theory as $k_L = C_V v_s^2 \tau/3$. The low thermal conductivity in bulk bismuth telluride is ascribed to the combination of low speed of sound and low acoustic cut-off energy[40] and yields 1.6 W m^{-1} K^{-1} at room temperature.[57] In this study, no change in the phonon lifetime was identified and thus was assumed the same between bulk and Bi_2Te_3 NW. The heat capacity at constant volume, C_v, in bulk Bi_2Te_3 essentially reaches the Dulong–Petit limit at 295 K.[40] Given that only tiny differences are seen in the Te specific density of phonon states between bulk and Bi_2Te_3 nanowires, at 295 K, which is above the Debye temperature, similar C_v is reasonably expected. However, a 6.5% decrease in the average speed of sound has been identified in 56 nm diameter nearly stoichiometric Bi_2Te_3 NW compared to the bulk counterpart. Thus, in the first approximation, due to the quadratic dependence of thermal conductivity on the speed of sound, a reduction of 13% is expected with respect to the bulk value. A decrease between 28 and 57% in the macroscopically measured thermal conductivity was reported[54] for similar diameter but different stoichiometry nanowires, *i.e.* $Bi_{0.485}Te_{0.515}$, as well as for mechanically exfoliated stacks of Bi_2Te_3 thin films and ribbons.[58–61] The macroscopically available data do not match our prediction. However, in macroscopic studies lattice thermal conductivity is not measured directly but is extracted from a combination of measurements – *i.e.* macroscopic thermal conductivity and electrical conductivity – and assumptions, *i.e.* estimation of the Lorentz number, *L*, in the Wiedemann–Franz law. Experimental artifacts and theoretical concerns have been invoked, notably that the Lorentz number in the Wiedemann–Franz law is significantly lower for low dimensional structures[62,63] compared to bulk samples. Thus, in order to further clarify the contribution of nanostructuration in macroscopic thermal conductivity combined microscopic and macroscopic measurements as a function of diameter and composition are required.

5 Conclusions

Microscopic lattice dynamic measurements on an array of 56 nm diameter nearly stoichiometric Bi_2Te_3 nanowires using nuclear inelastic scattering by ^{125}Te have been reported. We demonstrate a robust way of measuring the speed of sound in nanowires. No effect related to confined dimensions in the phonon lifetime has been measured. The extracted density of phonon states shows that nanostructuration leads to a reduction in the speed of sound as compared to the bulk counterpart which is predicted to result in a 13% reduction in the lattice part of thermal conductivity. Thus, nanostructuration indeed favourably impacts properties required for the thermoelectric and phase change applications.

Acknowledgements

The DFG priority program SPP1386 'Nanostructured Thermoelectrics' is acknowledged for the financial support of this study. R.H. acknowledges support from the Helmholtz – University Young Investigator Group "Lattice Dynamics in Emerging Functional Materials". RH and DB acknowledge the European Synchrotron Radiation Facility for provision of synchrotron radiation beam time and the helpful discussions with Dr A. Chumakov and Dr R. Rüffer during data acquisition at ID18. Also the Advanced Photon Source for provision of synchrotron radiation beam time and the help of Dr D. Robinson during data acquisition at 6-ID-D is acknowledged.

References

1 G. C. Schatz, *Proc. Natl. Acad. Sci. U. S. A.*, 2007, **104**, 6885.
2 A. A. Balandin, *Nat. Mater.*, 2011, **10**, 569.
3 B. Poudel, Q. Hao, Y. Ma, Y. Lan, A. Minnich, B. Yu, X. Yan, D. Wang, A. Muto, D. Vashaee, X. Chen, J. Liu, M. S. Dresselhaus, G. Chen and Z. Ren, *Science*, 2008, **320**, 634.
4 V. Swamy, E. Holbig, L. S. Dubrovinsky, V. Prakapenka and B. C. Muddle, *J. Phys. Chem. Solids*, 2008, **69**, 2332.
5 A. K. Geim and K. S. Novoselov, *Nat. Mater.*, 2007, **6**, 183–191.
6 C. Lee, I. Kim, H. Shin, S. Kim and J. Cho, *Nanotechnology*, 2010, **21**, 185704.
7 T. Gao and T. Wang, *Cryst. Growth Des.*, 2010, **10**, 4995–5000.
8 L. D. Hicks and M. S. Dresselhaus, *Phys. Rev. B: Condens. Matter*, 1993, **47**, 12727.
9 L. D. Hicks and M. S. Dresselhaus, *Phys. Rev. B: Condens. Matter*, 1993, **47**, 16631.
10 P. S. Kireev, *Semiconductor Physics*, Mir Publishers, 1978.
11 A. Balandin and K. L. Wang, *Phys. Rev. B: Condens. Matter*, 1998, **58**, 1544–1549.
12 A. Balandin and K. L. Wang, *J. Appl. Phys.*, 1998, **84**, 6149–6153.
13 J. Zou and A. Balandin, *J. Appl. Phys.*, 2001, **89**, 2932–2938.
14 J. E. Cornett and O. Rabin, *Appl. Phys. Lett.*, 2011, **98**, 182104.
15 M. Kashiwagi, S. Hirata, K. Harada, Y. Zheng, K. Miyazaki, M. Yahiro and C. Adachi, *Appl. Phys. Lett.*, 2011, **98**, 023114.
16 S. H. Lee, W. Shim, S. Y. Jang, J. W. Roh, P. Kim, J. Park and W. Lee, *Nanotechnology*, 2011, **22**, 295707.
17 A. A. Balandin and D. L. Nika, *Mater. Today*, 2012, **15**, 266–275.
18 N. Han, S. I. Kim, J.-D. Yang, K. Lee, H. Sohn, H.-M. So, C. W. Ahn and K.-H. Yoo, *Adv. Mater.*, 2011, **23**, 1871.
19 J. Liu, S. Liu and J. Wei, *Appl. Phys. Lett.*, 2010, **97**, 261903.
20 M. H. R. Lankhorst, B. W. S. M. M. Ketelaars and R. A. M. Wolters, *Nat. Mater.*, 2005, **4**, 347.
21 T. Matsunaga, N. Yamada, R. Kojima, S. Shamoto, M. Sato, H. Tanida, T. Uruga, S. Kohara, M. Takata, P. Zalden,

G. Bruns, I. Sergueev, H. C. Wille, R. P. Hermann and M. Wuttig, *Adv. Funct. Mater.*, 2011, **21**, 2232.
22 C. Weber, A. Fuhrer, C. Fasth, G. Lindwall, L. Samuelson and A. Wacker, *Phys. Rev. Lett.*, 2010, **104**, 036801.
23 C.-L. Hsin, M. Wingert, C.-W. Huang, H. Guo, T.-J. Shih, J. Suh, K. Wang, J. Wu, W.-W. Wu and R. Chen, *Nanoscale*, 2013, **5**, 4669–4672.
24 P. N. Martin, Z. Aksamija, E. Pop and U. Ravaioli, *Nano Lett.*, 2010, **10**, 1120–1124.
25 I. Campbell and P. Fauchet, *Solid State Commun.*, 1986, **58**, 739–741.
26 X. Wang, A. Shakouri, B. Yu, X. Sun and M. Meyyappan, *J. Appl. Phys.*, 2007, **102**, 014304.
27 A. I. Chumakov, A. Q. R. Baron, R. Rüffer, H. Grünsteudel, H. F. Grünsteudel and A. Meyer, *Phys. Rev. Lett.*, 1996, **76**, 4258.
28 H.-C. Wille, R. P. Hermann, I. Sergueev, U. Pelzer, A. Möchel, T. Claudio, J. Perßon, R. Rüffer, A. Said and Y. V. Shvyd'ko, *Europhys. Lett.*, 2010, **91**, 62001.
29 K. Nielsch, J. Choi, K. Schwirn, R. B. Wehrspohn and U. Gsele, *Nano Lett.*, 2002, **2**, 677.
30 L. Trahey, C. R. Becker and A. M. Stacy, *Nano Lett.*, 2007, **7**, 2535–2539.
31 N. Peranio, E. Leister, W. Töllner, O. Eibl and K. Nielsch, *Adv. Funct. Mater.*, 2012, **22**, 151–156.
32 L. Fuentes-Montero, M. E. Montero-Cabrera and L. Fuentes-Cobas, *J. Appl. Crystallogr.*, 2011, **44**, 241–246.
33 N. Peranio, E. Leister, W. Töllner, O. Eibl and K. Nielsch, *J. Electron. Mater.*, 2012, **41**, 1509.
34 N. Peranio and O. Eibl, *Phys. Status Solidi A*, 2007, **204**, 3243.
35 I. Sergueev, H.-C. Wille, R. P. Hermann, D. Bessas, Y. V. Shvyd'ko, M. Zajac and R. Rüffer, *J. Synchrotron Radiat.*, 2011, **18**, 802.
36 R. Rüffer and A. Chumakov, *Hyperfine Interact.*, 1996, **97–98**, 589.
37 V. Kohn and A. Chumakov, *Hyperfine Interact.*, 2000, **125**, 205–221.
38 H. J. Lipkin, *Phys. Rev. B: Condens. Matter*, 1995, **52**, 10073–10079.
39 S. Nakajima, *J. Phys. Chem. Solids*, 1963, **24**, 479–485.
40 D. Bessas, I. Sergueev, H.-C. Wille, J. Persson, D. Ebling and R. Hermann, *Phys. Rev. B: Condens. Matter*, 2012, **86**, 224301.
41 A. I. Chumakov, R. Rüffer, A. Q. R. Baron, H. Grünsteudel, H. F. Grünsteudel and V. G. Kohn, *Phys. Rev. B: Condens. Matter*, 1997, **56**, 10758–10761.
42 A. Chumakov and W. Sturhan, *Hyperfine Interact.*, 1999, **123–124**, 781.
43 M. Y. Hu, W. Sturhahn, T. S. Toellner, P. D. Mannheim, D. E. Brown, J. Zhao and E. E. Alp, *Phys. Rev. B: Condens. Matter*, 2003, **67**, 094304.
44 T. B. Massalski, Binary Alloys Phase Diagrams, *Am. Soc. Met.*, 1990, **1**, 800–801.
45 H. Lind, S. Lidin and U. Häussermann, *Phys. Rev. B: Condens. Matter*, 2005, **72**, 184101.
46 H. Lind and S. Lidin, *Solid State Sci.*, 2003, **5**, 47–57.
47 C.-N. Liao, H.-D. Shih and P.-W. Su, *J. Electrochem. Soc.*, 2010, **157**, D605–D608.
48 D. L. Medlin, Q. M. Ramasse, C. D. Spataru and N. Y. C. Yang, *J. Appl. Phys.*, 2010, **108**, 043517.
49 D. Abdula, K. T. Nguyen, K. Kang, S. Fong, T. Ozel, D. G. Cahill and M. Shim, *Phys. Rev. B: Condens. Matter*, 2011, **83**, 205419.
50 J. O. Jenkins, J. A. Rayne and R. W. Ure, *Phys. Rev. B: Condens. Matter*, 1972, **5**, 3171.
51 A. A. Balandin, E. P. Pokatilov and D. Nika, *J. Nanoelectron. Optoelectron.*, 2007, **2**, 140–170.
52 S. Davis and G. Gutirrez, *J. Phys.: Condens. Matter*, 2011, **23**, 495401.
53 D.-A. Borca-Tasciuc and G. Chen, *J. Appl. Phys.*, 2005, **97**, 084303.
54 J. Zhou, C. Jin, J. H. Seol, X. Li and L. Shi, *Appl. Phys. Lett.*, 2005, **87**, 133109.
55 J. Fleurial, L. Gailliard, R. Triboulet, H. Scherrer and S. Scherrer, *J. Phys. Chem. Solids*, 1988, **49**, 1237–1247.
56 A. Jacquot, N. Farag, M. Jaegle, M. Bobeth, J. Schmidt, D. Ebling and H. Böttner, *J. Electron. Mater.*, 2010, **39**, 1861–1868.
57 D. Spitzer, *J. Phys. Chem. Solids*, 1970, **31**, 19–40.
58 V. Goyal, D. Teweldebrhan and A. A. Balandin, *Appl. Phys. Lett.*, 2010, **97**, 133117.
59 D. Teweldebrhan, V. Goyal and A. A. Balandin, *Nano Lett.*, 2010, **10**, 1209–1218.
60 K. M. F. Shahil, M. Z. Hossain, D. Teweldebrhan and A. A. Balandin, *Appl. Phys. Lett.*, 2010, **96**, 153103.
61 D. Teweldebrhan, V. Goyal, M. Rahman and A. A. Balandin, *Appl. Phys. Lett.*, 2010, **96**, 053107.
62 F. Völklein, H. Reith, T. W. Cornelius, M. Rauber and R. Neumann, *Nanotechnology*, 2009, **20**, 325706.
63 J. Kimling, S. Martens and K. Nielsch, *Rev. Sci. Instrum.*, 2011, **82**, 074903.